



# Numerical Simulation of Effect Modification of Single Slotted Flap on Wing Cessna C208B Grand Caravan for Aerodynamic Performance

Septian Yusuf<sup>(✉)</sup>, Setyo Hariyadi, and Nyaris Pambudiyatno

Politeknik Penerbangan Surabaya, Jemur Andayani I/73, Wonocolo Surabaya,  
Jawa Timur 60236, Indonesia

septianyusuf2000@gmail.com

**Abstract.** A wing through which fluid flows will form a three-dimensional separation caused by two interacting boundary layers. This separation will result in secondary flow which can be detrimental to airfoil performance. Until now, aircraft often use a slotted type flap that can prevent separation so that it can reduce the value of less resistance. This study will examine the performance and aerodynamic characteristics of the modified single-slotted flap on the Cessna 208b Grand Caravan wing. The method used is a numerical simulation with CFD software in the form of ANSYS. The test object is a modified Cessna 208b Grand Caravan wing with a single slotted flap with a flap angle ( $\alpha_F$ ) of  $0^\circ$ ,  $15^\circ$ , and  $30^\circ$  to determine the effect of aerodynamic performance. The angles of attack reviewed are  $\alpha = 0^\circ, 2^\circ, 4^\circ, 6^\circ, 8^\circ, 10^\circ, 12^\circ, 14^\circ, 15^\circ, 16^\circ, 18^\circ$ , and  $20^\circ$ . The fluid flow used is air with a cruising speed of 96 m/s above sea level in stable conditions. The simulation results show that the addition of flap angle modification on the Cessna C208b Grand Caravan wing can affect both performance and aerodynamic characteristics. At a speed of 96 m/s, increasing the flap angle can decrease the value of  $C_L/C_D$  at high angles of attack. However, the addition of the flap angle can provide a better  $C_L/C_D$  value at low angles of attack.

**Keywords:** single slotted flap · CFD · lift · drag · lift-to-drag ratio

## 1 Introduction

A wing through which fluid flow passes will form a three-dimensional separation caused by two interacting boundary layers. This separation will result in secondary flow which can be detrimental to airfoil performance. This loss is in the form of a reduced effective area that can generate lift [1]. The flap is the most common high lift device used in airplanes. The flap allows a compromise between high cruise speed and low landing speed as it can be extended when needed and retracted into the wing structure when not needed. at this time, aircraft often use a slotted type flap can prevent separation to reduce the value of the drag force which is less.

One method that is often used to support research on aerodynamics at this time is Computational Fluid Dynamic (CFD). Computational Fluid Dynamics is a science that

studies how to predict fluid flow patterns, heat transfer, chemical reactions, and other phenomena by solving mathematical equations or mathematical models by utilizing computer computational assistance to perform calculations on each divisor element [2]. This study aims to determine how the effect of single slotted flap modification on the Cessna C208b Grand Caravan wing on the coefficient of lift ( $C_L$ ), coefficient of drag ( $C_D$ ), and the comparison of values  $C_L/C_D$  as well as the characteristic of contour visualization of pressure, velocity, and vorticity magnitude to the angle of attack.

Some experts who have examined the dynamics of fluid flow in slotted flaps include Kasim [3], Chapman [4], Foster [5], Velkova [6, 7], and others. Todorov [8] conducted research single slotted flaps for light airplane wings. The method that will be used in this study is a two-dimensional numerical simulation using fluent software. The test object is in the form of airfoil NACA 23012 with a chord length of 1m, and flap deflection angle of  $0^\circ$  to  $20^\circ$ . Fluid flow configuration is Reynolds number ( $Re$ ) =  $3 \times 10^6$  in steady conditions. From this study, CFD results were obtained for the proposed wing single slotted flap configuration showing a higher lift coefficient compared to the airfoil NACA 23012 baseline and the wing-single plain flap configuration. The drag coefficient is smaller than a single-wing configuration. From this study, CFD results were obtained for the proposed wing-single slotted flap configuration showing a higher lift coefficient compared to the airfoil NACA 23012 baseline and the wing-single plain flap configuration. The drag coefficient is smaller than the wing with a single plain flap configuration.

This study shows how the effect of the single slotted flap modification on the Wing Cessna C208B Grand Caravan on the  $C_L$  and  $C_D$  and the lift-to-drag ratio value. In addition, this study also showed a comparison of visualization of contour pressure coefficient, velocity, and vorticity magnitude of the single slotted flap on wing Cessna C208B Grand Caravan.

## 2 Method

The research method in this study uses a three-dimensional numerical simulation method. The software used is Ansys Fluent with a turbulent model using K- $\epsilon$  Realizable. The simulation process can be divided into three parts, namely: Pre-processing, processing, and post-processing. The test object uses a Cessna C208b Grand Caravan wing with dimensions of 1:1 to the actual dimensions and flap geometry based on Todorov's research [8] so that the results obtained can be validated.

### 2.1 Simulation Domain and Boundary Condition

A model that represents the test object is called a domain. The determination of the domain must be adjusted to ideal conditions to get the appropriate results [9]. In this case, the domain is a wing in the test section in the form of a wind tunnel. For all boundary conditions, it can be seen in Fig. 1. At the inlet, the boundary conditions used are 96 m/s or the aircraft cruising speed. The simulation domain is compiled based on Mulvany [10] and Hariyadi's research [11] with the area behind the trailing edge as far as 5 chord lines (Figs. 2 and 3).

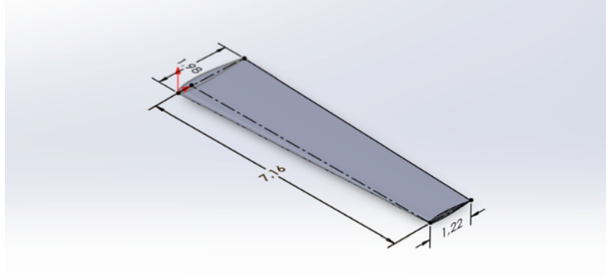


**Fig. 1.** Wing geometry in simulation

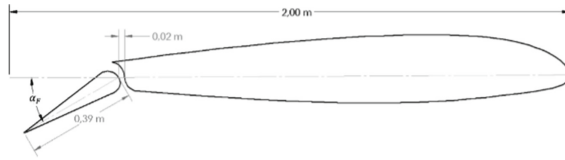


**Fig. 2.** Single-slotted flap geometry in simulation

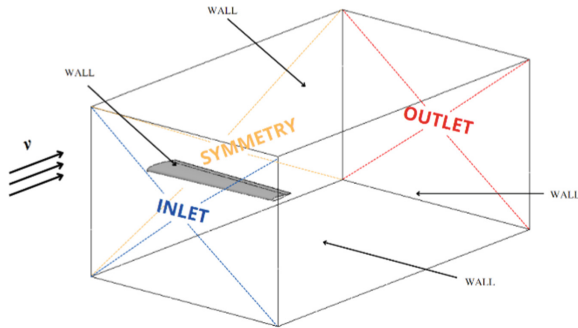


**Fig. 3.** Simulation Domain and Boundary Condition

## 2.2 Grid Independence Test

The use of simulation software requires data accuracy both at the pre-processing and post-processing stages. The grid-independent test stage is needed to find out and determine the most efficient grid structure and level for modeling results close to the actual conditions [12]. This independent grid test is carried out for meshing which tends to be constant, the number of meshing is divided into several types, then from this type of meshing the smallest value of each meshing will be found by comparing numerical  $C_D$  graphs.

The number of meshing is divided into 10 types. Table 1 shows the comparison of the values  $C_D$  generated from ten types of meshing. One of the considerations used in a numerical simulation is a low and constant  $C_D$  value. So in this simulation, Mesh 5 will be used as a reference for the next simulation according to Anderson's [13] criterion.

**Table 1.** Grid Independence Test Analysis on Test Object without Flap

Jenis Mesh	Element	Node	Drag (N)	$C_D$
Meshing 1	2973528	536344	551.932	0.007103
Meshing 2	3144327	567622	551.113	0.007093
Meshing 3	3342603	603273	552.029	0.007105
Meshing 4	3579492	646215	554.961	0.007142
Meshing 5	3985830	719004	552.925	0.007116
Meshing 6	4345541	783368	553.072	0.007118
Meshing 7	4776373	861801	554.978	0.007027
Meshing 8	5308558	957603	554.463	0.007156
Meshing 9	5830581	1049415	551.257	0.007002
Meshing 10	6472375	1090534	552.242	0.007157

### 3 Result and Discussion

This result will be discussed through the coefficient of lift, coefficient of drag, and coefficient of lift-to-drag ratio. In addition, it also discusses the visualization of the contour coefficient pressure, velocity, and vorticity magnitude. So based on the analysis of the numerical simulation results, the aerodynamic performance and its characteristics will be obtained.

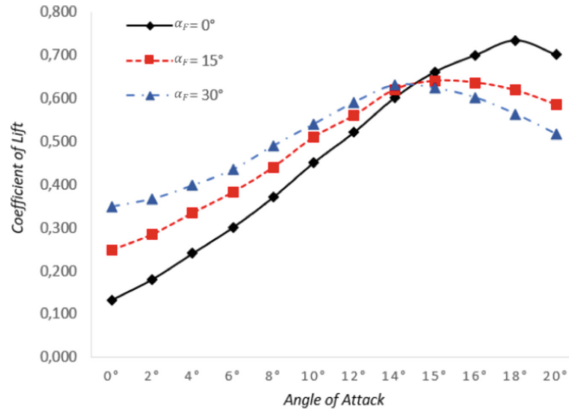
#### 3.1 Coefficient of Lift

Figure 4 shows a graph between the coefficient of lift and the angle of attack at the flap angle ( $\alpha_F$ ) = 0°, 15°, and 30°. It can be seen that the flap angle has a significant effect on the  $C_L$  value of the wing Cessna 208b Grand Caravan.

Comparison of the  $C_L$  values of the flap angle ( $\alpha_F$ ) 0°, 15°, and 30° to the angle of attack provides information that an increase in the flap angle can increase production at a low angle of attack. However, increasing the flap angle can reduce the maximum  $C_L$ . It can be seen that the variation  $\alpha_F = 0^\circ$  can produce the highest maximum  $C_L$  value than other variations, which is 0.7336. And experienced the longest loss of lift or stall, which occurred at  $\alpha_F = 18^\circ$ . While the lowest maximum  $C_L$  value is generated by variation  $\alpha_F = 30^\circ$ , which is 0.630 at  $\alpha_F = 14^\circ$ . Even though it produces the lowest maximum  $C_L$  value, this variation can produce a greater  $C_L$  value than the variation at a low angle of attack.

#### 3.2 Coefficient of Drag

Figure 5 shows the graph between  $C_D$  and the angle of attack on the variation of the flap angle ( $\alpha_F$ ) positioned at 0°, 15°, and 30°. The graph has provided information that the flap angle has a significant effect on the  $C_D$  value of the Cessna 208b Grand Caravan wing.



**Fig. 4.** Lift coefficient at Flap Angle ( $\alpha_F$ ) 0°, 15°, and 30°

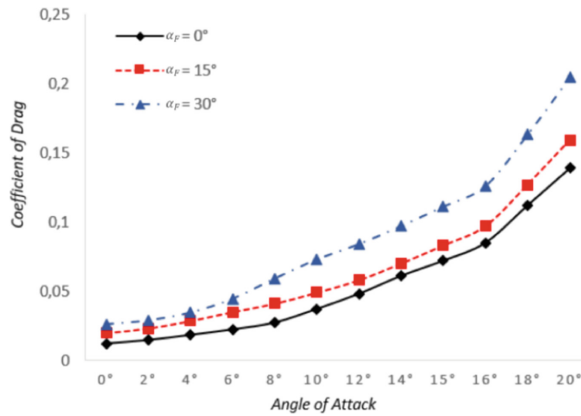


**Fig. 5.** Drag coefficient at Flap Angle ( $\alpha_F$ ) 0°, 15°, and 30°.

The addition of the flap angle also affects the  $C_D$  value significantly. It can be seen that the use of an  $\alpha_F = 30^\circ$  flap angle produces the highest  $C_D$  value. This indicates that the greater the addition of the flap angle, the more the resulting  $C_D$  value will increase. This pattern is similar to the research conducted by Hussein et al. [14]. This is caused by increasing the flap angle, the greater the outer cross-section which is perpendicular to the direction of airflow.

### 3.3 Lift to Drag Ratio

Figure 6 shows a graph between  $C_L/C_D$  and the angle of attack at various flap angles ( $\alpha_F$ ) positioned at 0°, 15°, and 30°. It can be seen that the variation of the flap angle 0° produces the largest  $C_L/C_D$  value of 13.65 when the angle of attack is at 8°. And at the angle of attack after that, the performance decreased due to the addition of the resulting drag force. While the variation of the 15° flap angle, continues to decrease in

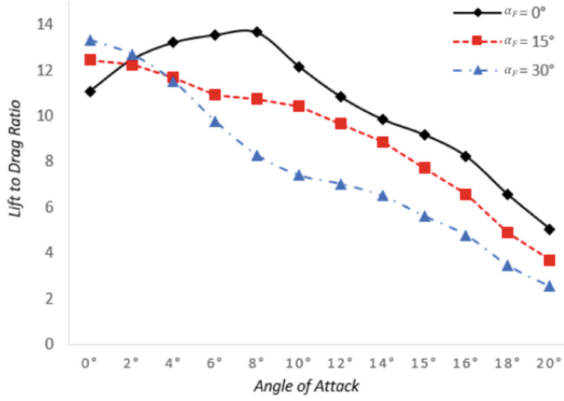


**Fig. 6.** Lift to Drag ratio at Flap Angle ( $\alpha_F$ )  $0^\circ$ ,  $15^\circ$ , and  $30^\circ$

value  $C_L/C_D$  as the angle of attack increases. However, the  $\alpha_F = 15^\circ$  flap angle variation can produce a value  $C_L/C_D$  better than the  $\alpha_F = 0^\circ$  at the  $0^\circ$  angle of attack. The same pattern occurs in the  $\alpha_F = 30^\circ$  flap angle with a value of  $C_L/C_D$  higher than the  $\alpha_F = 15^\circ$  flap angle. Therefore, the flap angle of  $\alpha_F = 30^\circ$  is good to use during take-off flight conditions because it produces the most optimal  $C_L/C_D$  value at a  $0^\circ$  angle of attack.

The graph shows that the use of flap angle can affect the value of  $C_L/C_D$  generated. Although the use of flaps can provide an additional  $C_L$  value, the  $C_D$  value will also increase as the flap angle used increases. At a low angle of attack, the addition of the flap angle has helped to generate additional lift which increases the value of  $C_L/C_D$ . However, as the angle of attack increases, the value of  $C_L/C_D$  continues to decrease due to the increase in the resulting drag.

### 3.4 Velocity Contour

When the flap angle is positioned at  $\alpha_F = 15^\circ$  with the same angle of attack, there is an increase in the velocity difference between the top and bottom surfaces. This causes the addition of the  $C_L$  value as well as  $C_D$ . And when the flap angle is increased to  $\alpha_F = 30^\circ$ , airflow and turbulent separation occur only at the top of the flap. The point of airflow separation is depicted by a dark blue contour with a certain area. Meanwhile, turbulent flow is indicated by an irregular streamlined direction. This is due to the increasing cross-sectional area perpendicular to the direction of the airflow so that the momentum of the incoming airflow through the gap cannot delay the separation point.

The comparison of the wing with the flap angle positioned at  $\alpha_F = 30^\circ$  can be identified by three angles of attack, namely  $\alpha = 0^\circ$ ,  $8^\circ$ , and  $16^\circ$ . At an angle of attack of  $\alpha = 0^\circ$ , there is little point of separation or turbulent flow. This is depicted by a blue contour area located in the upper area of the flap. When the angle of attack is positioned at  $\alpha = 8^\circ$ , the airflow separation area is slightly widened to the center of the top surface of the wing. However, the characteristics of the streamlined direction have not shown significant difference from the  $\alpha = 0^\circ$  angle of attack. And when the angle of attack is positioned at  $\alpha_F = 30^\circ$ , there are significant differences that occur in both contour color

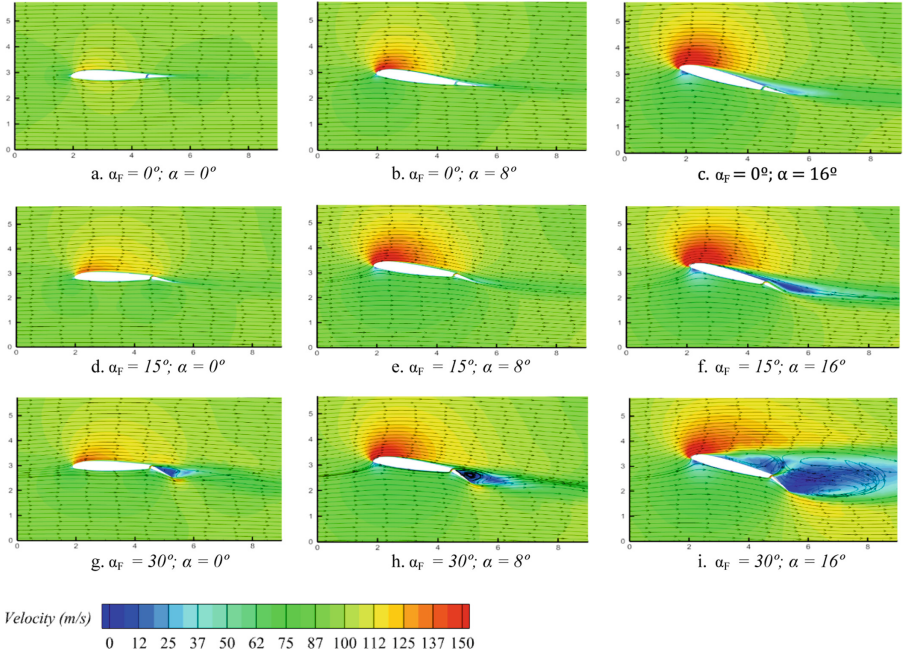


**Fig. 7.** Velocity contour at Wing Cessna 208b Grand Caravan with Variasi Single Slotted Flap

and streamline characteristics. The area of airflow separation is widened to occur in the maximum chamber airfoil and is followed by turbulent flow in the blue contour area. Meanwhile, the momentum of the airflow entering the gap from the flap is not able to delay the separation point.

Based on the simulation results, it can be seen that the addition of the flap angle greatly affects the aerodynamic characteristics of the high angle of attack. The larger the flap angle used, the greater the separation. The point of stagnation is getting further away from the leading edge as the angle of attack increases. However, with increasing the flap angle for the same angle of attack, the flow separation increases significantly. For  $\alpha_F = 0^\circ$  flap angle, the flow separation (blue zone on the left) at an angle of attack of  $\alpha = 16^\circ$  is less than that of  $\alpha_F = 15^\circ$  and  $30^\circ$  flap angle (Fig. 7).

### 3.5 Pressure Coefficient Contour

The pressure contour in Fig. 8 changes as the flap angle increases. The most significant area of pressure change is the leading edge area on the upper surface airfoil. This event is explained by variation  $\alpha_F = 30^\circ$ ;  $\alpha = 16^\circ$  which experienced a significant difference in pressure between the leading edge and trailing edge of the wing surface. With the flaps that are deflected by  $15^\circ$  and  $30^\circ$ , it seems as if the velocity at the bottom of the airfoil is slowed, while at the top of the airfoil the fluid velocity is accelerated resulting in a low-pressure coefficient in that area. Where the leading edge of the airfoil is blue and the trailing edge is red.

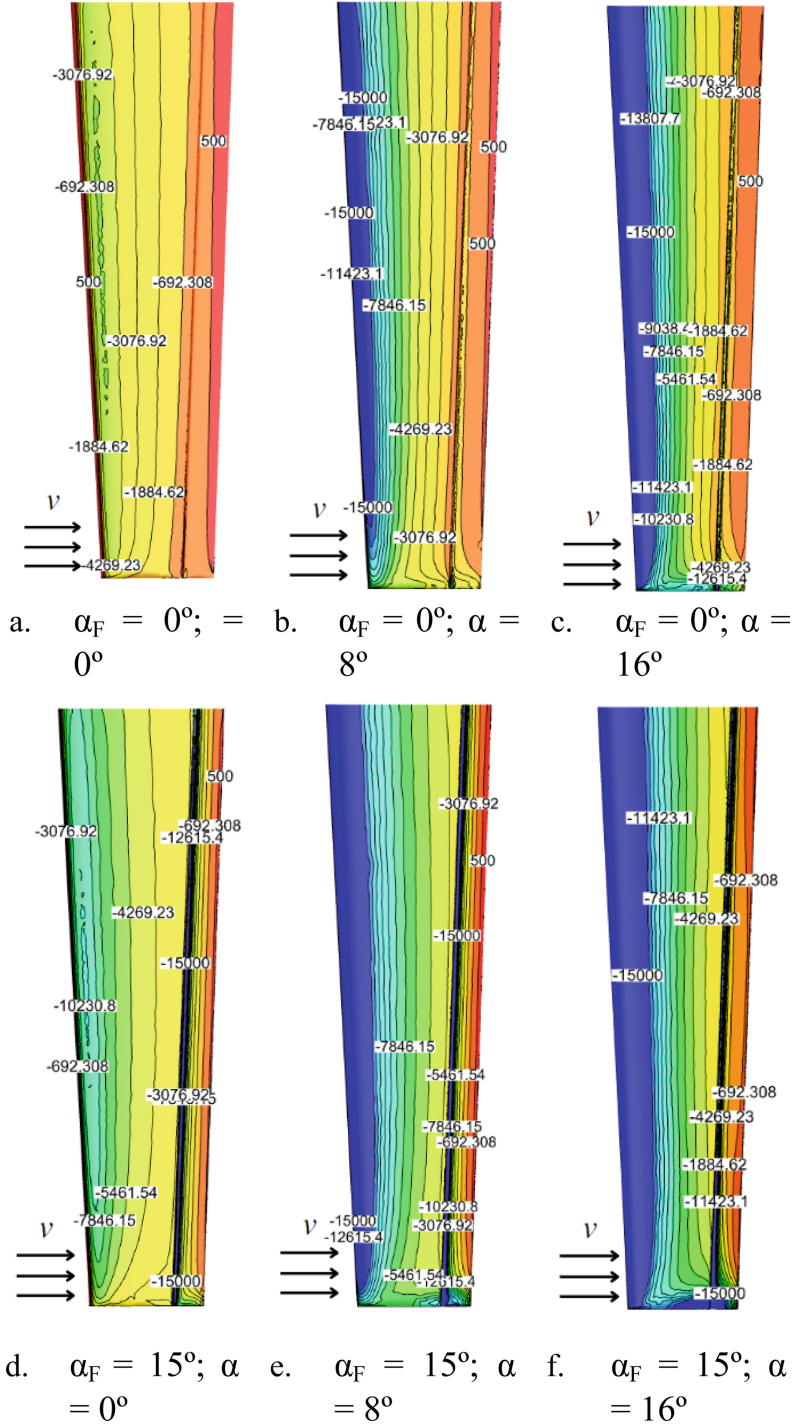


**Fig. 8.** Pressure Coefficient Contour on the Cessna 208b Grand Caravan wing with single slotted flap variation



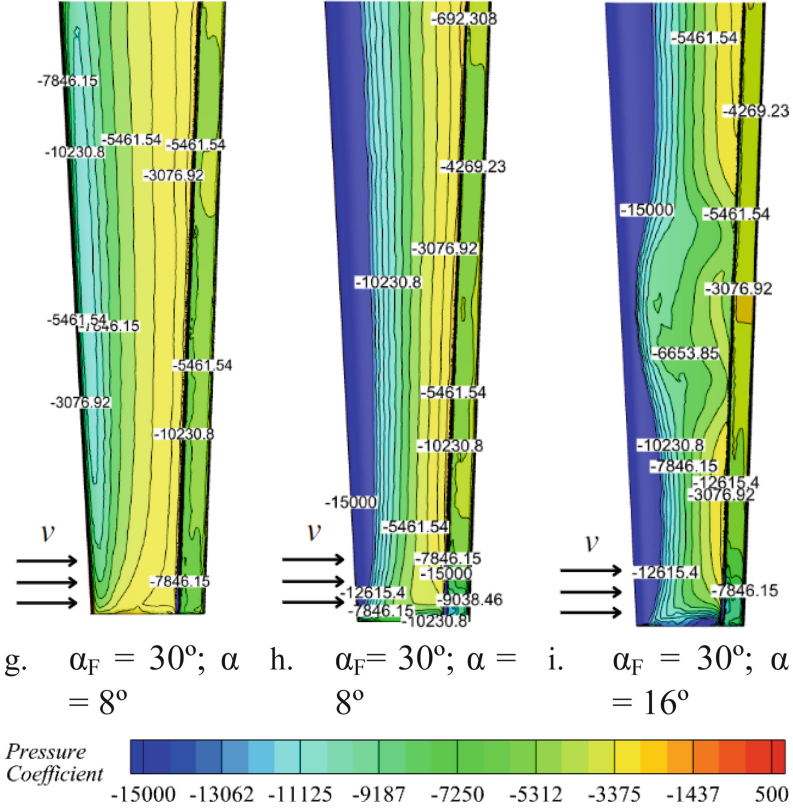
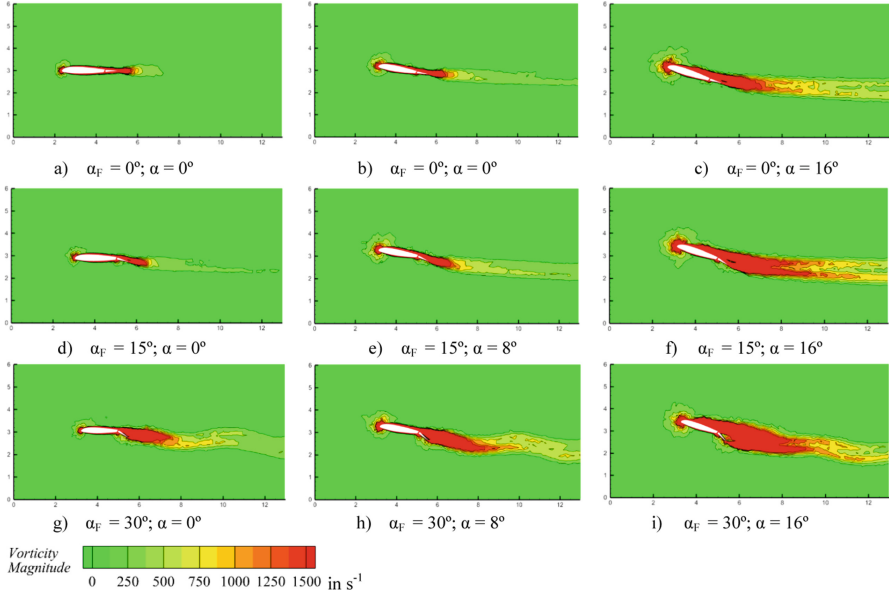


Fig. 8. (continued)

At  $\alpha = 16^\circ$  with the flap angle positioned to  $\alpha_F = 0^\circ$ , there is a low-pressure formation in the leading edge area which is shown in solid blue. However, when the flap angle is positioned at  $\alpha_F = 15^\circ$  the low-pressure area widens and an increase in pressure occurs in the trailing edge area. And when the flap angle is enlarged to  $\alpha_F = 30^\circ$  there is an expansion of the minimum pressure area with inconsistent contours. This indicates the occurrence of airflow separation or large turbulence experienced by the airflow after passing through the wing surface. The existence of these events is reinforced by significant impairment in  $C_L$  value.

### 3.6 Vorticity Magnitude Contour

In Fig. 9, the contours of the vorticity magnitude are shown by flap angles of  $\alpha_F = 0^\circ$ ,  $15^\circ$ , and  $30^\circ$  and angles of attack at  $\alpha = 0^\circ$ ,  $8^\circ$ , and  $16^\circ$  in the midspan wing area. The red contour shows a high vorticity value while the green color indicates a low vorticity value. At a flap angle of  $\alpha_F = 0^\circ$  and an angle of attack of  $\alpha = 0^\circ$ , strong vortices are formed with a length of less than half the chord length behind the wing. When the angle of attack is positioned at  $\alpha = 8^\circ$ , the area is extended.



**Fig. 9.** Vorticity Magnitude Contour on the Cessna 208b Grand Caravan wing with single slotted flap variation

Based on the simulation results, it provides information that the addition of the angle of attack and flap angle can produce varying induce drag. The higher the angle of attack or flap angle used, the greater the induced drag generated. This greatly affects the value.

## 4 Conclusion

Numerical simulation of the effect of single-slotted flap modification on the Cessna C208b Grand Caravan wing on aerodynamic performance resulted in the following conclusions.

1. Comparison of  $C_L$  values for flap angles  $\alpha_F = 0^\circ$ ,  $15^\circ$ , and  $30^\circ$  to the angle of attack provides information that increasing flap angle can increase  $C_L$  production at a low angle of attack. However, increasing the flap angle can reduce the maximum  $C_L$ .
2. The addition of the flap angle also significantly affects the  $C_D$  value. It can be seen that the use of an  $\alpha_F = 30^\circ$  flap angle produces the highest  $C_D$  value. This indicates that the greater the addition of the flap angle, the more the resulting  $C_D$  value will increase.
3. Although the use of flaps can provide additional  $C_L$  value, the  $C_D$  value will also increase as the flap angle used increases. At a low angle of attack, the addition of the flap angle has helped to generate additional lift which increases the value of  $C_L/C_D$ . However, as the angle of attack increases, the value of  $C_L/C_D$  continues to decrease due to the increase in the resulting drag

4. The pressure contour changes as the flap angle increases. The most significant areas of pressure changes are the leading edge and upper surface areas, especially the maximum chamber airfoil.
5. The larger the flap angle used, the greater the separation. The point of stagnation is getting further away from the leading edge as the angle of attack increases. However, with increasing the flap angle for the same angle of attack, the flow separation increases significantly.
6. Based on the simulation results, it provides information that the addition of the angle of attack and flap angle can produce varying induced drag. The higher the angle of attack or flap angle used, the greater the induced drag generated. This greatly affects the value of the  $C_D$

## References

1. J. Duncan, Pilot 's Handbook of Aeronautical Knowledge, Pilot. Handb. Aeronaut. Knowl. (2016) 524.
2. J.D. Anderson, Fundamentals of Aerodynamics (6th edition), McGraw-Hill, 2011.
3. K. Biber, Stall Hysteresis of an Airfoil with Slotted Flap, 42 (2005).
4. J. Chapman, Numerical Investigation of Flow Characteristics of a Slotted NACA 4414 Airfoil Numerical Investigation of Flow Characteristics of a Slotted NACA 4414 Airfoil, (2019).
5. D. Foster, H. Irwin, B. Williams, The Two-Dimensional Flow Around a Slotted Flap, Aeronaut. Res. Counc. Reports Memo. 3681. (1971).
6. C. Velkova, M. Todorov, Study of The Influence of A Gap between The Wing and Slotted Flap on The Aerodynamic Characteristics of Ultra-Light Aircraft Wing Airfoil, (2015).
7. C. Velkova, M. Todorov, G. Durand, Study the Influence of a Gap between the Wing and Slotted Flap over the Aerodynamic Characteristics of Ultra-Light Aircraft Wing Airfoil, 5 (2015) 278–285. <https://doi.org/10.17265/2159-5275/2015.05.002>.
8. M.D. Todorov, Aerodynamic Characteristics of Airfoil with Single Slotted Flap for Light Airplane Wing, (2015).
9. S.P. Setyo Hariyadi, Sutardi, W.A. Widodo, I. Sonhaji, Numerical Study of Secondary Flow Characteristics on the Use of the Winglets, J. Phys. Conf. Ser. 1726 (2021). <https://doi.org/10.1088/1742-6596/1726/1/012012>.
10. N. Mulvany, L. Chen, J. Tu, B. Anderson, Steady-State Evaluation of Two-Equation RANS (Reynolds-Averaged Navier-Stokes) Turbulence Models for High-Reynolds Number Hydrodynamic Flow Simulations, Dep. Defence, Aust. Gov. (2004) 1–54.
11. S.P.S. Hariyadi, B. Junipitoyo, Sutardi, W.A. Widodo, Stall Behavior Curved Planform Wing Analysis with Low Reynolds Number on Aerodynamic Performances of Wing Airfoil Eppler 562, J. Mech. Eng. 19 (2022) 201–220.
12. S.P. Setyo Hariyadi, Sutardi, W.A. Widodo, M.A. Mustaghfirin, Aerodynamics Analysis of the Wingtip Fence Effect on UAV Wing, Int. Rev. Mech. Eng. 12 (2018). <https://doi.org/10.15866/ireme.v12i10.15517>.
13. J.D. Anderson, J.D. Anderson Jr, Computational Fluid Dynamics The Basics with Applications, 1995. <https://doi.org/https://doi.org/10.1017/CBO9780511780066>.
14. E.Q. Hussein, H.N. Azziz, F.L. Rashid, Aerodynamic Study of Slotted Flap for Naca 24012 Airfoil by Dynamic Mesh Techniques and Visualization Flow, J. Therm. Eng. 7 (2021) 230–239. <https://doi.org/10.18186/THERMAL.871989>.

**Open Access** This chapter is licensed under the terms of the Creative Commons Attribution-NonCommercial 4.0 International License (<http://creativecommons.org/licenses/by-nc/4.0/>), which permits any noncommercial use, sharing, adaptation, distribution and reproduction in any medium or format, as long as you give appropriate credit to the original author(s) and the source, provide a link to the Creative Commons license and indicate if changes were made.

The images or other third party material in this chapter are included in the chapter's Creative Commons license, unless indicated otherwise in a credit line to the material. If material is not included in the chapter's Creative Commons license and your intended use is not permitted by statutory regulation or exceeds the permitted use, you will need to obtain permission directly from the copyright holder.

